Competitive effect of the metallic canister and clay barrier on the sorption of Eu^{3+} under subcritical conditions

Said El Mrabet[1], Miguel A. Castro[1], Santiago Hurtado[2], M. Mar Orta[1], M. Carolina Pazos[1], María Villa-Alfageme [3] and María D. Alba[1†]

[1]Instituto Ciencia de Materiales de Sevilla (CSIC-Universidad de Sevilla).
Avda. Américo Vespucio, 49. 41092 Sevilla, Spain

[2] Servicio de Radioisótopo del CITIUS (Universidad de Sevilla).
Avda. Reina Mercedes, 4. 41012 Sevilla, Spain

[3] Dpt. Física Aplicada II (Universidad de Sevilla).
Avda. Reina Mercedes, s/n. 41012 Sevilla, Spain

Abstract

An in depth knowledge and understanding of high activity radionuclide (HLRW) immobilization processes on the materials composing the engineered barrier (clay and metallic canister) is required to ensure the safety and the long-term performance of radioactive waste disposal procedures. Therefore, the aim of this study was to understand the mechanisms involved in the retention of Eu^{3+} by two components of the multibarrier system, the bentonite barrier and the canister. As such, a comparative study of the interaction of trivalent Eu^{3+}, used to simulate trivalent actinides, with both bentonite and a metallic canister has been undertaken in this work. To this end, we designed a minireactor into which the bentonite was introduced and compacted. The minireactor-bentonite system was then submitted to a hydrothermal reaction with a $7.9 \cdot 10^{-2}$ M solution of Eu^{3+} at 300ºC for 4.5 days. SEM and XRD results revealed that

† *Corresponding author: E-mail: alba@icmse.csic.es*

both bentonite and the container were involved in the immobilization of europium by the formation of insoluble europium silicate phases. The presence of europium silicate adsorbed on the surface of the metallic canister indicates the competitive effect of both components of the engineered barrier (bentonite and metallic canister) in HLRW immobilization. These results suggested that the canister could play a role in the HLRW immobilization even during its corrosion process.

Keywords. Metallic canister, bentonite, engineering barrier, radionuclide waste, actinide, lanthanide, rare earth elements, silicates, hydrothermal treatment.

1. Introduction

The complexity of radioactive waste management is one of the most significant challenges faced by all countries involved in nuclear power generation. Likewise, it is also a concern in many other countries that use radioactive materials for medical, industrial, or research purposes. Much of this waste needs to be disposed of in ways that minimise its negative impact. In particular, the most hazardous and long-lived waste such as spent nuclear fuel or reprocessing waste arising from the operation and dismantling of nuclear reactors must be contained and isolated in order to ensure the long-term radiological protection of humans and the environment. Disposal of such waste in deep underground-geological repositories has become an effective and universally preferred option (Savage and Chapman, 1982; Allègre, 1999; McCombie et al., 2000). However, such disposal requires the design of an isolation system consisting of several barriers that are able to confine the radioactivity for a long period of time. Most such repository designs are based on a multi-barrier system consisting of two fundamental components, namely a natural and an engineered barrier (McCombie et al., 2000; Astudillo, 2001; Chapman, 2006). The engineered barrier includes a metallic container, whose main function is to confine the radionuclides in the waste package during the specified period and a backfill material, made up mainly of bentonite, that stands between the container and host rocks in order to prevent the access of groundwater to the HLRW waste and its subsequent migration to the geosphere (Bailey, 1980).

To improve the safety of the disposal system, each of those barriers alone should be able to protect the repository systems from water intrusion over its design lifetime and prevent the spread of hazardous radionuclides from the repository to the biosphere.

As such, container corrosion and the chemical interactions of corrosion products with the clay buffer are of great interest for the long-term performance of a repository (Wilson et al. 2006a and 2006b). After closure of the disposal repository, the low permeability of the clay surrounding the container means that it progressively becomes saturated with groundwater. The expected environment then becomes oxidizing due to the presence of dissolved oxygen in the water and air trapped in the near field (Spink and Wood, 1990). Once the oxygen trapped in the repository has been consumed entirely, the canister undergoes anaerobic corrosion, thus resulting in the generation of hydrogen and iron-corrosion products from the canister such as magnetite (Fe_3O_4), and goethite (FeO(OH)) (Smart et al.2002; Carlson et al. 2007). Siderite ($FeCO_3$) is also formed under the expected geological conditions for groundwater with high concentrations of CO_3^{2-} ions and in the presence of compacted clay; iron silicates such as berthierine may also be important (Ishidera et al. 2008; Savage et al., 2010). Ultimately, the canister may be perforated as a result of such corrosion processes, thus allowing radionuclide migration through the clay buffer via diffusion and retardation by sorption within the clay (Xia et al., 2005). Most of the iron diffuses from the container into the surrounding barrier (bentonite), where it precipitates and subsequently induces deterioration of the buffer barrier, a process that may result in a loss of some crucial properties of bentonite such as swelling capacities and sorption. Carlson et al. (2007) have reported increased hydraulic conductivity due to interaction with steel corrosion products.

Several studies concerning the corrosion of candidate metals for the container, as well as the interaction of their corrosion products with bentonite, have been reported in the literature (Guillaume et al. 2004; Perronnet et al. 2004; Chuanhe et al. 2011). Likewise, systematic destabilization of the smectite to non-swelling sheet silicates when

in contact with iron metal and/or iron oxides has been extensively investigated (Guillaume et al. 2003, 2004, Perronnet et al. 2004, Lantenois et al. 2005; Wilson et al. 2006a and 2006b). Thus, Lantenois et al. (2003) carried out experiments with different smectites in order to determine the effect of crystallo-chemical features on the smectite/ iron interactions. At 80°C, the results indicated that oxidation of the container by smectites occurs only for dioctahedral smectites under basic pH conditions, whereas the container corrodes by precipitating magnetite, but without smectite alteration, at pHs ranging from slightly acid to neutral. Iron/clay interactions have also been modelled, and it has been shown that most of the Fe diffuses from the canister into the bentonite, where it sorbs or precipitates as magnetite (Samper et al. 2008). Detailed mineralogical analysis of corrosion experiments by Milodowski et al. (2009a; 2009b) tends to suggest other solid products.

As far as steel-bentonite interactions are concerned, the transformation of bentonite into other minerals, as a result of its interaction with the corrosion products of metallic container, has been observed (Julien et al 2005, Bildstein et al. 2006). These corrosion products, together with the high pH value produced at the container-clay interface and in the host rock, result in smectite destabilization and precipitation of magnetite, hematite, goethite and serpentine-like minerals, thus resulting in the loss of some of the bentonite properties, such as its swelling and cation-exchange capacity (Bildstein et al., 2006; Carlson et al., 2007; Gaudin et al., 2009; Savage et al., 2010). The effect of container corrosion on the stability of clay mineral therefore depends mainly on factors such as pH, temperature, the crystal chemistry of the clay; the water/solid ratio and the iron/clay mass (Gaudin et al., 2009).

Few studies of concerning the role of the backfill material in the kinetics and mechanism of container corrosion have been conducted to date. An understanding of the sorption/retention of radionuclides on the materials used to construct the engineered barrier (clay and container waste) is therefore imperative in order to be able to adequately assess the long-term performance of radioactive waste disposal facilities. Likewise, very few studies have been carried out to evaluate the active participation of the metal container in the retention of radioactive waste. In this sense, Parfitt et al. (1980) studied the adsorption of Eu^{3+} by the metallic container and showed that the presence of free iron oxides inhibits adsorption of Eu^{3+} on the clay surface. Moreover, the adsorption of Eu^{3+} in hematite was found to be inhibited at pH> 5 in the presence of organic matter (Fairhurst et al. 1995, Rabung et al. 1998). Similarly, Quinn et al. (2006) found that the adsorption constant of various rare earth elements on the surface of hematite is related to the physicochemical properties of these rare earth cations. Davranche et al. (2004) studied sorption of the entire rare earth element (REE) series onto iron oxyhydroxide, in the presence of humic acid, the observation of Yttrium (YREE) sorption pattern was interpreted in terms of complexation with humate that was dissolved in solution and sorbed onto hematite (Fairhurst et al., 1995; Rabung et al., 1998b; Davranche et al., 2004). Philippini et al (2006) studied the sorption of silicon on various corrosion products such as magnetite Fe_3O_4, goethite (α-FeOOH), siderite ($FeCO_3$) and pyrite (FeS_2) and found that only three of the four studied corrosion products are able to sorb silicon but in different proportions whereas the sorption capacity by pyrite was estimated negligible.

Several studies have been undertaken to determine the ability of magnetite, commonly formed on corroding steel surfaces, to absorb or reduce some radionuclides (Granizo and Missana, 2006; Rovira et al., 2004). Savage et al. (2010) observed that

Magnetite occurs as a transitory phase, which may explain the very thin layers of magnetite in some recent experimental studies of steel corrosion in compacted bentonite.

In light of the above, this paper aims to study the competitiveness of bentonite and the metal canister for retaining radioactive actinides. In this work, ^{152}Eu was selected to simulate trivalent actinides, Bentonite FEBEX material, as simulator of the materials of the engineered barrier and the austenitic stainless steel 316L as simulator of the metallic canister material (J. M. Gras, 2002; ENRESA, 2004).

2. Methods

2.1. Experimental design and materials

The clay mineral used in this study (Bentonite FEBEX) has been extensively investigated in the recent past in many countries in Europe and around the word (Tripathy et al., 2004). This bentonite was provided by the ENRESA Company (the Spanish Company in charge of radioactive wastes management) and had the structural formula ($(Ca_{0.5}Na_{0.08}K_{0.11})(Si_{7.78}Al_{0.22})(Al_{2.78}Fe^{3+}_{0.33}Fe^{2+}_{0.02}Mg_{0.81})O_{20}(OH)_4$.). Its main mineralogical component is montmorillonite (smectite percentage higher than 90%) together with small amounts of quartz (Fernandez et al., 2004).

Europium nitrate $Eu(NO_3)_3 \cdot 4.88H_2O$, which is commercially available from Sigma-Aldrich, was used as the rare earth element source, as Eu^{3+} is commonly used as a trivalent actinide analogue due to their chemical similarity (Chapman and Smellie, 1986; Buil et al., 2007).

A wide variety of metallic materials have been investigated as candidates for the disposal of radioactive waste. Copper, titanium, stainless steels were found to be suitable materials because they exhibit a high resistance attack in the expected disposal environment (Rebak, 2006). Therefore, in the present study, hydrothermal experiments were carried out in a stainless steel AISI-316 L reactor, (chosen as candidate container), commercially available, the chemical composition is given in Table 1, and the design in Fig. 1a.

In order to understand the competitive effect of the container material in the processes by which the bentonite clay retains radioactive waste, a minireactor made from the same material as the steel reactor was designed by us. Thus, 300 mg of the powdered bentonite was placed into a cylindrical steel cell (minireactor) 8 mm in diameter and 2 mm in height (Fig. 1a). The bentonite-minireactor set was then compacted in a cylindrical die at a pressure of 4 tonnes for 5 min. Finally, the compacted set was placed into the steel reactor and submitted to a hydrothermal reaction with 40 mL of $7.9 \cdot 10^{-2}$ M Eu^{3+} solution, this concentration allows that Eu^{3+} was not a limiting reagent (Alba et al., 2011), at 300 ºC for 4.5 days. Despite, the expected temperature in the disposal repositories which will not exceed 150ºC, many studies have been carried out by simulating the deep geological disposal at temperatures up to 350ºC to increase the reaction rate (Mather et al., 1982; Savage and Chapman., 1982; Allen and Wood, 1988, Alba and Chain., 2007). Alba et al. (2009; 2011) observed that similar chemical reaction between lanthanide cations and clays occurred at lowest temperature but after longer reaction time.

To discriminate between the effect of the canister-bentonite competitiveness and the effect of the hydrothermal treatment, a blank treatment was carried out. Thus, the

minireactor was submitted to a similar hydrothermal treatment but without bentonite and europium solution.

2.2. Characterization methods

The X-ray diffraction patterns were obtained using an X'Pert Pro PANALYTICAL diffractometer in the conventional $\theta - 2\theta$ Bragg–Brentano configuration using Cu Kα radiation. Diffractograms were registered from 3º to 70º 2θ and in steps of 0.05º. The morphology and chemical composition of both the steel and bentonite before and after hydrothermal treatment with the rare earth solution at 300ºC for 4.5 days were investigated using a SEM-FEG HITACHI S- 4800 a scanning electron microscope equipped with an Xflash 4010 (BRUKER) for energy dispersive X-ray (EDX) analysis. The pH of the supernatant was measured at room temperature using a Eutech Instruments PC 700 pH-meter before and after the hydrothermal treatment in aerobic conditions.

3. Results and Disscussion

3.1. Sorption of Eu^{3+} on Bentonite FEBEX

Fig. 1 shows a comparative visual analysis of the system (minireactor and bentonite) before and after the hydrothermal treatment. The visual analysis of the bentonite after hydrothermal treatment at 300ºC for 4.5 days in the presence of europium (Fig. 1b) showed the typical spongy appearance of clay.

Fig. 2 shows the XRD pattern of the bentonite before and after treatment with a solution of $7.9 \cdot 10^{-2}$ M Eu^{3+} at 300ºC for 4.5 days. The XRD pattern of untreated

bentonite (Fig. 2a) has been included for reference. Montmorillonite remains the main constituent of the bentonite after hydrothermal treatment, although the quartz is now absent. This treatment provokes a 001 space expansion from 1.39 nm to 1.51 nm that can be explained by the sorption of hydrated M^{3+} cations into the interlayer space (Alba et al., 2001). It is in good agreement with the previous studies which reported that the hydrothermal treatment of bentonite in the presence of the canister does not decrease its swelling capacity (Bildstein et al., 2006; Carlson et al., 2007; Gaudin et al., 2009; Savage et al., 2010).

The 060 reflection of untreated and treated FEBEX at 62.0º 2θ which correspond to a b-spacing value of 1.495 Å, is typical of their dioctahedral character (Davidtz and Low 1970). The absence of a shift in this reflection to a higher 2θ angle, and therefore lower b-spacing, indicates that there is not leaching of the octahedral cations (Grim, 1968) as would be expected as a result of hydrothermal treatment at acid pH, Table 2, (Corma et al. 1987; Komadel 1996).

Finally, it is remarkable that no phases resulting from minireactor degradation, or europium silicate bearing phases were detected in the reacted bentonite.

The SEM micrographs of FEBEX before and after hydrothermal treatment are shown in Fig. 3. The SEM micrograph of untreated bentonite (Fig. 3a) shows the typical lamellar morphology for the most particles. Furthermore, the typical $K_{\alpha 1}$ lines for Si, Mg, Al and Ca in montmorillonite can be seen in the corresponding EDX spectrum (Fig. 4). In contrast, although the SEM micrographs of the reacted bentonite (Fig. 3b-d) also show a lamellar morphology for most particles, the associated EDX spectrum shows the typical $K_{\alpha 1}$ lines for Si, Mg and Al of bentonite, $L_{\alpha 1}$ and $L_{\beta 1}$ lines of Eu are also observed which indicate that the spectrum was compatible with smectite with Eu^{3+}

as interlayer cations (Fig. 4d, ③). Together with these lamellar particles, and under the backscattering electron beam, agglomerations of small particles as well as other block morphologies with a chemical composition associated to the newly formed europium crystalline phase were also observed (labelled ② and ① respectively in Fig. 3d). The corresponding EDX spectra were characterised by the $K_{\alpha 1}$ lines of Si, Al, Mg and the L_{α} and L_{β} lines of Eu. No free Mg and Al spectra were found because of the contribution of electrons arising from bentonite particles. Likewise, no K_{α} or K_{β} spectral lines for the Fe, which can be released upon degradation of the minireactor, were detected.

3.2. Sorption of Eu^{3+} on the minireactor

Visual analysis of the minireactor after hydrothermal treatment at 300ºC for 4.5 days in the presence of bentonite and europium (Fig. 1b) showed that the steel surface was entirely covered by a thin, compact dark-red layer, thus indicating that the hydrothermal process had somehow affected the minireactor´s surface.

The dominant peaks in the X-ray diffraction pattern of the minireactor after blank hydrothermal treatment at 300°C for 4.5 days (Fig. 5a) are due to the original austenitic metallic matrix of the steel, thus implying that the minireactor did not undergo any noticeable change in term of microstructure as a result of the hydrothermal treatment. However, after treatment with bentonite and Eu^{3+} at 300 ºC for 4.5 days, the XRD pattern (Fig. 5b) showed a similar, but much weaker, austenitic signal for the metallic steel matrix which indicates that the oxide layer formed on the surface was somewhat thicker. Additionally, a considerable portion of europium silicate, $Eu_2Si_2O_7$ (PDF 00-23-247) and Eu_3SiO_5 (PDF 00-20-403), from the mixed europium nitrate-bentonite solution was observed in the XRD diagram. Minor phases, such as, halloysite ($Al_2Si_2O_7 \cdot xH_2O$, PDF 00-02-229), n=β-$NaAl_7O_{11}$ (PDF 00-21-1095), and, j=jadeite

1 ($NaAlSi_2O_6$, PDF 00-22-1338), which contain elements leached from bentonite, were
2 also detected.

3 The SEM micrograph of the minireactor surface submitted to the blank treatment
4 shows that the surface is entirely covered by a thin layer of fine oxide crystals (Fig.6 b).
5 Likewise, the EDX spectrum (Fig. 7b) only shows the spectral lines of the austenitic
6 phase, similar to that of the untreated steel (Fig. 7a), although the prominent spectral
7 line for oxygen indicates a partial oxidation of the reactor surface during the
8 hydrothermal process. The absence of any new crystalline phase by XRD (Fig. 5a)
9 indicates that the oxidation of the surface generated amorphous phases.

10 The SEM micrographs of the minireactor after hydrothermal treatment with
11 bentonite and europium solution (Fig. 6c-f) revealed that the reactor surface is covered
12 by small crystals on which large crystals have grown. According to the EDX analysis,
13 the small crystals (Fig. 7e-f) have a similar composition to the large crystals but with
14 higher europium content (Fig. 7d), probably due to the size difference between the
15 crystals. It should be noted that the electron beam penetrated the small crystal
16 completely, thus implying higher concentrations of silicon and europium. In general, the
17 crystals were Si- and Eu-rich, with varying Eu/Si intensity ratios.

18 In order to gain a deeper insight into the diffusion of europium into the
19 minireactor and the distribution of the chemical elements in the oxide layer formed after
20 the hydrothermal treatment, a detailed cross-sectional study involving SEM
21 observations in combination with an EDX line profile along a representative area (white
22 line in Fig. 8a) of the minireactor was performed. This study showed an enrichment of
23 Eu and Si corresponding to europium silicate at the scale-atmosphere interface with a
24 thickness of ca. 5 μm (Fig 8b). The silicon and europium signals decreased

progressively as the alloy was reached. In agreement with the results obtained by surface SEM analysis, there was no evidence of europium diffusion towards the metallic container.

3.3. Supernatant characterization

The physicochemical characteristic of the initial solution and supernatant (Table 2) shows that the initial pH value decreased from 4.72 to about 2, thus indicating an acidic medium for the supernatant solution. This acidic condition explain why the bentonite was not affected by minireactor corrosion, as predicted by Lantenois et al. (2005) who found that the destabilization of smectites in contact with metallic Fe at a pH lower than 7 was not significant.

The conductivity showed a general increase in solution even when part of the europium had precipitated out of solution to form a solid phase. This can be explained by leaching of cations, mainly sodium or calcium released by an ion-exchange process.

The Pourbaix diagram (Fig. 9) allows the chemically stable europium along the pH-Redox potential (Eh) plot to be predicted. This plot shows that the E_h and pH values measured for both solutions favour europium as Eu^{3+} ions in water as an ideal solution.

4. Conclusions

The present work, has demonstrated that both bentonite and the metal container are involved in the immobilization of the reactive element europium through on specific

(precipitation, complexation and structural defect sorption) and nonspecific (cation-exchange interaction) sorption and chemical reaction.

The interaction between europium and bentonite involves both sorption at the cation-exchange sites located in the interlayer spaces of the clay (adsorption in no specific site) and chemical interaction with the generation of new phases such as $Eu_2Si_2O_7$ and Eu_3SiO_5. The formation of these phases on the engineered barrier (bentonite barrier) implies that this could be an efficient fail-safe mechanism for radioactive waste confinement when the suitable properties of bentonite such as swelling capacity and cation exchange failed to retain the radionuclide. The interaction of europium with the minireactor was only superficial and no europium diffusion towards the metallic container was detected.

These findings regarding the active participation of both components of the engineering barrier in the sorption of Eu^{3+} under subcritical conditions are in contrast to those of Parfitt (1980), who reported that free iron oxides reduce the sorption capacity of whole soil by coating the clay minerals in red earth thereby suppressing Eu^{3+} sorption. By means of XRD pattern, Europium silicate phases originated from the mixed solution of bentonite, Eu^{3+} and container were detected on the container surface but not observed in the bentonite due to their small crystalline domain size. Therefore, the metallic canister not only does not inhibit the formation of those phases from the bentonite but they are adsorbed onto the metallic canister surface which plays an active role in the HLRW immobilization, even in corrosion medium.

Acknowledgements

We are grateful for financial support from ENRESA (contract nº 0079000121) and from DGICYT and FEDER funds (Projects CTQ2010-14874).

References

Alba, M.D., Becerro, A.I., Castro, M.A., Perdigón, A.C., 2001. Hydrothermal reactivity of Lu-saturated smectites: Part I. A long-range order study. Am. Mineral., 86, 115-123.

Alba, MD., Chain, P., 2007. Persistence of lutetium disilicate. Appl. Geochem., 22, 192-201

Alba, MD., Chain, P., Orta, MM, 2009. Rare-earth disilicate formation under Deep Geological Repository approach conditions. Appl. Clay Sci., 46, 63-68.

Alba, MD., Castro, MA., Chaín, P., Hurtado, S., Orta, MM., Pazos, MC., Villa, M., 2011. Interaction of Eu-isotopes with saponite as component of the engineered barrier, 52, 253-257.

Allègre, M., 1999. The deep geological repository: an unavoidable and ethically correct solution. Proceedings of the 24-th Annual International Symposium, London.

Allen, C.C, Wood, M.I., 1988. Bentonite in nuclear waste disposal: A review of research in support of the Basalt Waste Isolation Project. Appl. Clay Sci., 3, 11-30

Astudillo J., 2001. El almacenamiento geológico profundo de los residuos radiactivos de alta actividad. Principios básicos y tecnología. ENRESA, Madrid.

Bailey, S.W., 1980. Structures of layer silicates. In: Brindley, G.W., and Brown, G. (Eds.).Crystal Structures of Clay Minerals and their X-ray Identification. London: Mineralogical Society, Pp 1-123.

Bildstein, O., Trotignon, L., Perronnet, M., Jullien, M., 2006. Modelling iron-clay interactions in deep geological disposal conditions. Phys. Chem. Earth, 31, 618-625.

Buil, B., Gomez, P., Garralon, A., Turrero, M.J., 2007. Rare-earth elements: a tool for understanding the behavior of trivalent actinides in the geosphere. Mater. Res. Soc. Symp. Proc., 985, 437-442.

Carlson, L., Karnland, O., Oversby, V.M., Rance, A.P., Smart, N.R., Snellman, M., Vähänen, M., Werme, L.O., 2007. Experimental studies of the interactions between anaerobically corroding iron and bentonite. Phys. Chem. Earth., 32, 334-345.

Chapman, N., 2006. Geological disposal of radioactive waste – concept, status and trends. J. Iber. Geol., 32, 7-14.

Chapman, N., Smellie, J., 1986. Introduction and summary of the workshop: natural analogues to the conditions around a final repository for high-level radioactive waste. Chem. Geol., 55, 167-173.

Chuanhe, Lu, Samper, J., Fritz, B., Clement, A., Montenegro, L., 2011. Interactions of corrosion products and bentonite: An extended multicomponent reactive transport model. Phys. Chem. Earth., 36, 1661-1668.

Corma, A., Mifsud, A., Sanz, E., 1987. Influence of the chemical-composition and textural characteristics of Palygorskite on the acid leaching of octahedral cations. Clay Minerals, 22, 225–232.

Davidtz, J.C., Low, P.F., 1970. Relation between crystal-lattice configuration and swelling of montmorillonites. Clays and Clay Minerals, 18, 325–332.

Davranche, M., Pourret, O., Gruau, G., Dia, A., 2004. Impact of humate complexation on the adsorption of REE onto Fe oxyhydroxide. *J. Colloid Interf. Sci.,* 277, 271–279.

ENRESA, 2004. Estudio de los productos de corrosión de la cápsula y su interacción con la barrera arcillosa de bentonita “CORROBEN”. Tech. Report (in Spanish)

Fairhurst, A.J., Warwick, P., Richardson, S., 1995. The influence of humic acid on the adsorption of europium onto inorganic colloids as a function of pH. Colloids Surfaces A. Physicochem. Eng. Aspects, 99, 187–199.

Fernandez, A., Baeyens, B., Bradbury, M., Rivas, P., 2004. Analysis of the porewater chemical composition of a Spanish compacted bentonite used in an engineered barrier. Phys. Chem. Earth., 29, 105-118.

Gaudin, A., Gaboreau, S., Tinseau, E., Bartier, D., Petit, S., Grauby, O., Foct, F., Beaufort, D., 2009. Mineralogical reactions in the Tournemire argillite after in-situ interaction with steels. Appl. Clay Sci., 43, 196-207.

Granizo, N., and Missana, T., 2006. Mechanisms of cesium sorption onto magnetite. Radiochim. Acta, 94, 671–677.

Gras, C.R, 2002. Lifeprediction for HLW containers – issues related to long-term extrapolation of corrosion resistance. Physique, 3, 891-902.

Grim, R.E., 1968. Clay Mineralogy. McGraw-Hill Book Company, New York.

Guillaume, D., Neaman, A., Cathelineau, M., Mosser-Ruck, R., Peiffert, C., Abdelmoula, M., Dubessy, J., Villiéras, F., Baronnet, A., Michau, N., 2003. Experimental synthesis of chlorite from smectite at 300 ºC in the presence of metallic Fe. Clay Miner., 38, 281–302.

Guillaume, D., Neaman, A., Cathelineau, M., Mosser-Ruck, R., Peiffert, C., Abdelmoula, M., Dubessy, J., Villiéras, F., Michau, N., 2004. Experimental study of the transformation of smectite at 80 and 300 ºC in the presence of Fe oxides. Clay Miner., 39, 17–34.

Ishidera, T., Ueno, K., Kurosawa, S., Suyama, T., 2008. Investigation of montmorillonite alteration and form of iron corrosion products in compacted

bentonite in contact with carbon steel for ten years. Phys. Chem. Earth. 33, S269-S275.

Jullien, M., Kohler, E., Raynal, J, Bildstein, O., 2005. Physicochemical reactivity in clay-rich materials: tools for safety assessment. Oil Gas Sci. Technol. Rev. IFP, 60, 107–120.

Komadel, P., Madejová, J., Janek, M., Gates, W.P., Kirkpatrick, R.J., Stucki, J.W., 1996. Dissolution of hectorite in inorganic acids. Clays and Clay Minerals, 44, 228–236.

Lantenois, S., 2003. Réactivité fer métal/smectites en milieu hydraté à 80°C. PhD thesis, Université d'Orléans, Orléans, France, 188 pp.

Lantenois, S., Lanson, B., Muller, F., Bauer, A., Jullien, M., Plançon, A., 2005. Experimental study of smectite interaction with metal Fe at low temperature: 1. Smectite destabilization. Clays Clay Miner., 53, 597-612.

Mather, J.D., Chapman, N.A., Black, J.H., Lintern, B.C., 1982. The geological disposal of high-level radioactive waste- a review of the Institute of geological sciences research-program. Nuclear energy-journal of the British nuclear energy society, 21, 167-173

McCombie, C., Pentz, D.L., Kurzeme, M., Miller, I., 2000. Deep geological repositories: a safe and secure solution to disposal of nuclear wastes. In GeoEng2000 – An international conference on geotechnical & geological engineering, 19-24 November 2000. Melbourne, Australia. Lancaster, Technomic.

Milodowski, A. E., Cave, M. R., Kemp, S. J., Taylor, H., Vickers, B., Green, K., Williams, C. L., and Shaw, R. A., 2009a. Mineralogical investigations of the interaction between iron corrosion products and bentonite from the NF-PRO

Experiments (Phase 1), SKB Technical Report TR-09-02, Swedish Nuclear Fuel and Waste Management Company, Stockholm, Sweden.

Milodowski, A. E., Cave, M. R., Kemp, S. J., Taylor, H., Green, K., Williams, C. L., Shaw, R. A., Gowing, C. J. B., and Eatherington, N. D., 2009b. Mineralogical investigations of the interaction between iron corrosion products and bentonite from the NF-PRO Experiments (Phase 2), SKB Report TR-09-03, Swedish Nuclear Fuel and Waste Management Company, Stockholm, Sweden.

Parfitt, R.L., 1980. Chemical properties of variable charge soils In: Theng, B.K.G. (ed.). Soils with Variable Charge. New Zealand Soc. Soil Sci., Bureau, Lower Hutt, pp. 167–194.

Perronnet, M., 2004. Réactivité des matériaux argileux dans un contexte de corrosion métallique. Application au stockage des déchets radioactifs en site argileux. PhD Thesis, Institut National Polytechnique de Lorraine, Nancy, France, p 283.

Philippini, V., Naveau, A., Catalette, H., Leclercq, S., 2006. Sorption of silicon on magnetite and other corrosion products of iron. J. Nucl. Mater., 348, 60-69.

Quinn, K.A., Byrne, R.H., Schijf, J., 2006. Sorption of yttrium and rare earth elements by amorphous ferric hydroxide: influence of pH and ionic strength. Mat. Chem., 99, 128–150.

Rabung, T., Geckeis, H., Kim, J.I., Beck, H.P., 1998. Sorption of Eu(III) on a natural hematite: application of a surface complexation model. J. Colloid Interf. Sci., 208, 153–161.

Rebak, R.B., 2006. Selection of Corrosion Resistant Materials for Nuclear Waste Repositories. Report of Lawrence Livermore National Laboratory, UCRL-PROC-221893.

Rovira, M., de Pablo, J., Casas, I., Giménez, J., and Clarens, F., 2004. Sorption of caesium on commercial magnetite with low silica content: experimental and modelling. Materials Research Symposium Proceedings, 807, 677–682.

Samper, J., Zheng, L., Fernández, A.M., Montenegro, L., 2008. Inverse modeling of multicomponent reactive transport through single and dual porosity media. Journal of Contaminant Hydrology, 98, 115–127.

Savage, D., Chapman, N.A., 1982. Hydrothermal behaviour of simulated waste glass- and waste-rock ineraction under repository conditions. Chemical Geology**,** 36, 59-86.

Savage, D., Watson, C., Benbow, S., Wilson, J., 2010. Modelling iron-bentonite interaction. Appl. Clay Sci.**,** 47, 91-98.

Smart, NR, Blackwood, DJ, Werme, L, 2002. Anaerobic corrosion of carbon steel and cast iron in artificial groundwaters: Part 1 – Gas generation. Corrosion. 58, 627-637.

Spinks, J.W.T., Wood, R.J., 1990. An Introduction to Radiation Chemistry, Third ed., John Wiley & Sons Inc., New York, 1990

Tripathy, S., Sriharan, A., Schanz, T. 2004. Swelling pressure of compacted bentonites from diffuse double layer theory. Can. J. Geotech., 41, 437-450.

Wilson, J., Savage, D., Cuadros, J., Shibata, M., Ragnarsdottir, K.V., 2006a. The efeect of iron on montmorillonite stability. (I). Background and thermodynamic considerations. Geochim. Cosmochim. Acta, 70, 306-322.

Wilson, J., Cressey, G., Cressey, B., Cuadros, J., Ragnarsdottir, K.V., Savage, D., Shibata, M., 2006b. The efeect of iron on montmorillonite stability. (II). Experimental investigation. Geochim. Cosmochim. Acta, 70, 323-336.

Xia, X., Idemitsu, K., Arima, T., Inagaki, Y., Ishidera, T., Kurosawa, S., Iijima K., Sato, H., 2005. Corrosion of carbon steel in compacted bentonite and its effect on neptunium diffusion under reducing condition. Applied Clay Science, 28, 89-100.

Table 1. Chemical composition (% by weight) of the stainless steel AISI 316 L used in this work

Co	V	Si	S	P	Mn	Cr	Fe	Ni	Cu	Mo	Cl
0.14	0.11	0.38	0.03	0.04	1.74	16.53	68.29	10.57	0.29	1.87	0.01

Table.2. Values of pH, redox potential (E_h) and conductivity of the initial aqueous solution and the solution after hydrothermal reaction at 300ºC for 4.5 days of FEBEX in contact with a solution of $7.9 \cdot 10^{-2}$M de Eu^{3+}.

solution	pH	E_h (mV)	Conductivity ($mS.cm^{-1}$)
initial	4.72	605	10.89
final	1.96	839	24.1

FIGURE CAPTIONS

Fig. 1. Illustrative picture of: a) the reactor and the minireactor used for the hydrothermal treatments, and, b) the bentonite FEBEX and the minireactor after being treated hydrothermally at 300ºC for 4.5 days in contact with a solution of $7.9 \cdot 10^{-2}$ M Eu^{3+} .

Fig. 2. XRD diffraction patterns of the bentonite FEBEX: a) untreated bentonite, and, b) after being treated at 300ºC for 4.5 days in contact with a solution of $7.9 \cdot 10^{-2}$ M Eu^{3+}. Q= quartz (PDF 00-01-649).

Fig. 3. a) SEM micrograph of the bentonite FEBEX. b) General view of the treated bentonite at 300ºC for 4.5 days in contact with a solution of $7.9 \cdot 10^{-2}$ M Eu^{3+}. c) and d) other zones from b) where small particles as well as block morphology are shown. Dots indicates the places where EDX analysis was performed

Fig. 4. EDX spectra of the different zones indicated in Fig. 3.d. EDX spectrum of the untreated bentonite FEBEX was included as reference.

Fig. 5. XRD diffraction patterns of the minireactor: a) after the blank hydrothermal treatment. b) after hydrothermal reaction with bentonite at 300ºC for 4.5 days in contact with a solution of $7.9 \cdot 10^{-2}$ M Eu^{3+}. A= austenite (PDF 00-33-397), *= $Eu_2Si_2O_7$ (PDF 00-23-247), += Eu_3SiO_5 (PDF 00-20-403), h= halloysite (PDF 00-02-229), n=β-$NaAl_7O_{11}$ (PDF 00-21-1095), and, j=jadeite (PDF 00-22-1338).

Fig. 6. SEM micrographs of the minireactor: a) as-made, b) after the blank hydrothermal treatment and, c-f) after hydrothermal reaction at 300ºC for 4.5 days with

bentonite FEBEX and a solution of $7.9 \cdot 10^{-2}$ M Eu^{3+}. Numbering levels indicate the particles where the EDX analysis was performed.

Fig. 7. EDX spectra of: a) as-made, b) after the blank hydrothermal treatment, and, c-e) after hydrothermal reaction at 300ºC for 4.5 days with bentonite FEBEX and a solution of $7.9 \cdot 10^{-2}$ M Eu^{3+}; zones 1, 2 and 3, respectively, indicated in Fig. 6.

Fig. 8. a) SEM micrograph of a transverse section of the minireactor after the reaction of the bentonite FEBEX with Eu^{3+} at 300ºC for 4.5 days. b) Intensity profile of the elemental composition.

Fig. 9. pH-Redox potential (Eh) plot (Pourbaix diagrams) of the initial $7.9 \cdot 10^{-2}$ M Eu^{3+} solution (circle) and the supernatant recovered after hydrothermal treatment (triangle).

Fig. 1

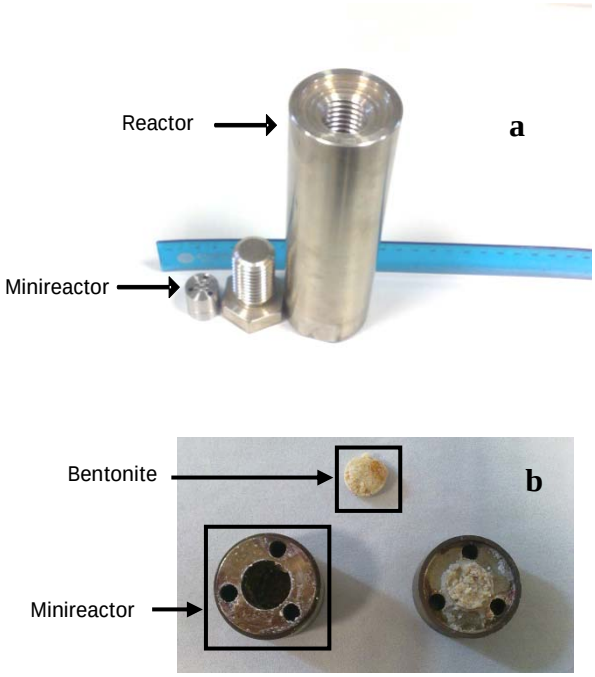

1
2
3
4

Fig. 2

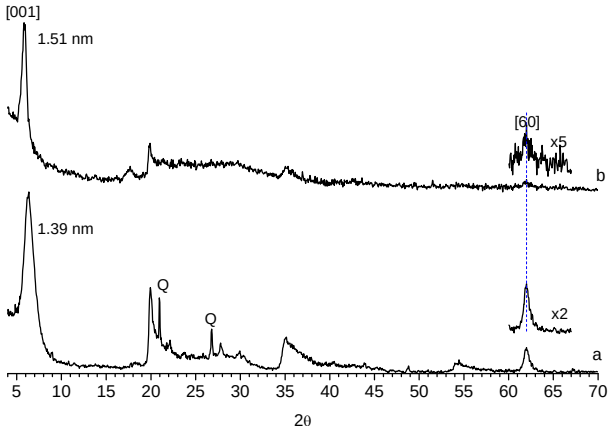
[001]
1.51 nm
[60]
x5
b
1.39 nm
Q
Q
x2
a
5
10
15
20
25
30
35
40
45
50
55
60
65
70
2θ

1
2 *Fig. 3*
3

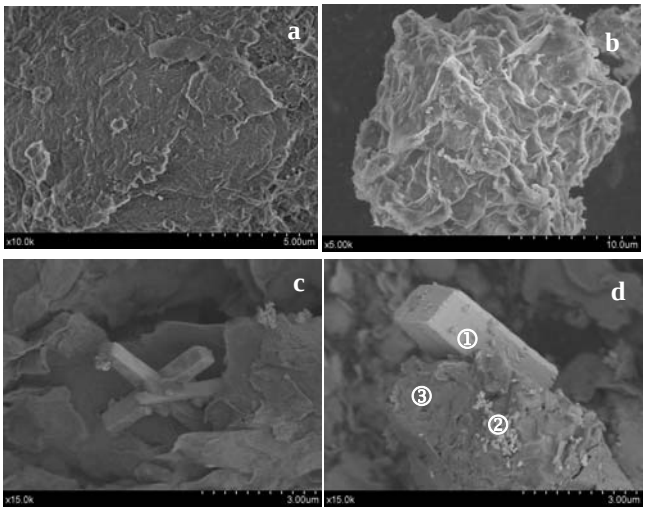

1 *Fig. 4*

2

3

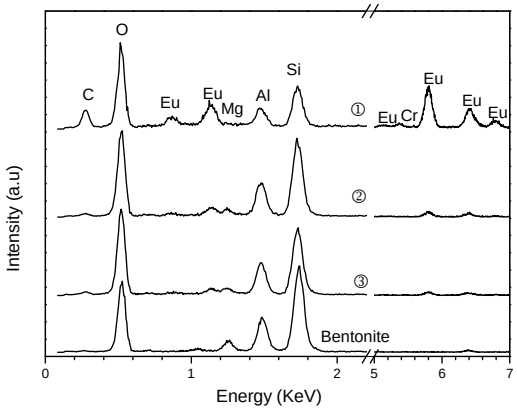
O
C
Eu
Eu
Mg
Al
Si
Eu
Eu
Cr
Eu
Eu
①
②
③
Bentonite
Intensity (a.u)
0
1
2
5
6
7
Energy (KeV)

Fig. 5

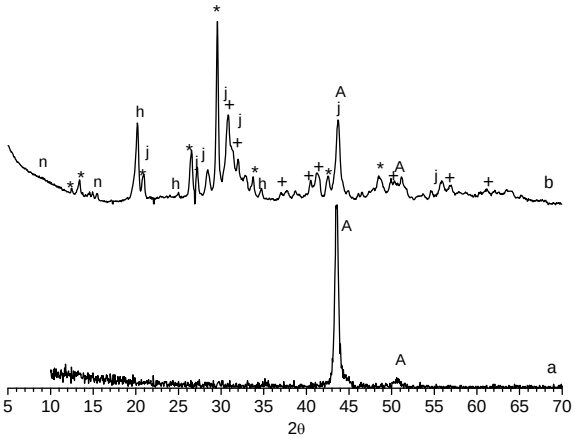

Fig. 6

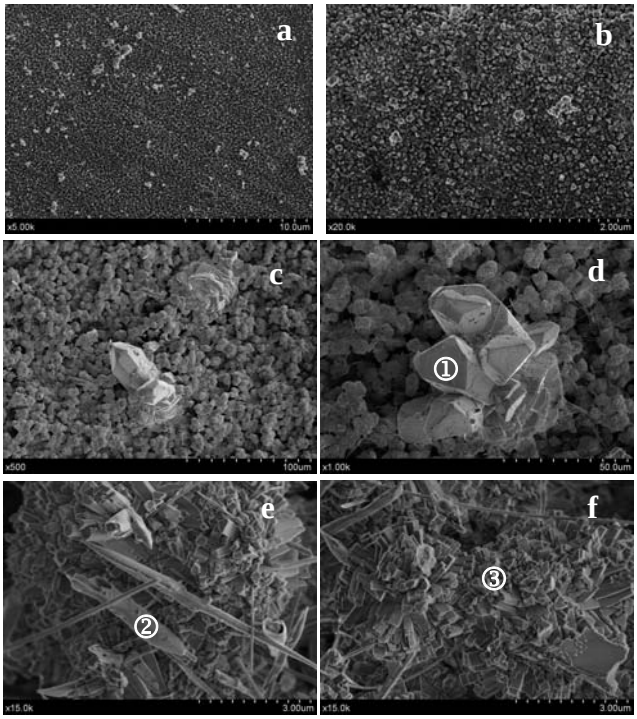

Fig. 7

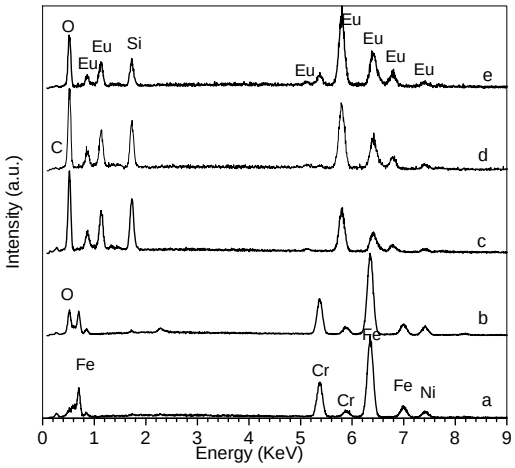
O
Eu
Eu
Si
Eu
Eu
Eu
Eu
Eu
e
C
d
c
O
b
Fe
Fe
Cr
Cr
Fe
Ni
a
Intensity (a.u.)
0
1
2
3
4
5
6
7
8
9
Energy (KeV)

1 *Fig. 8*

2

3

4

5

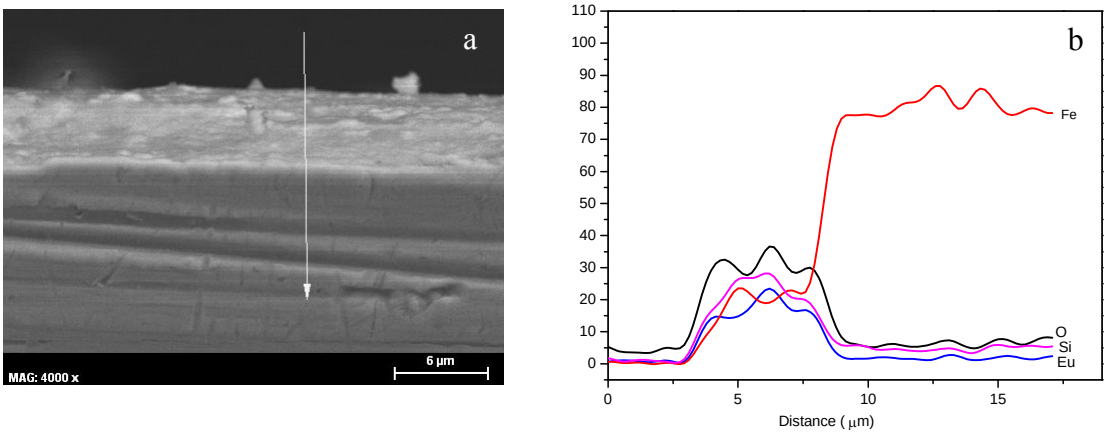
a
6 µm
MAG: 4000 x
b
110
100
90
80
70
60
50
40
30
20
10
0
0
5
10
15
Distance (µm)
Fe
O
Si
Eu

Fig. 9

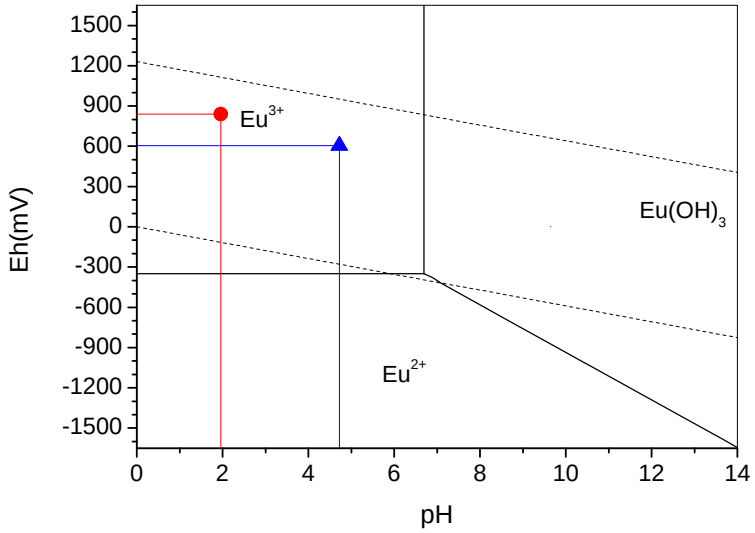
1500
1200
900
600
300
0
-300
-600
-900
-1200
-1500
Eh(mV)
0
2
4
6
8
10
12
14
pH
Eu3+
Eu2+
Eu(OH)3